Available online at www.sciencedirect.com
ScienceDirect
Catalysis Today 129 (2007) 79–85
CATALYSIS TODAY
www.elsevier.com/locate/cattod

Solar light assisted photodegradation of ethidium bromide over titania-based catalysts

C. Adán [a], A. Bahamonde [a,*], A. Martínez-Arias [a,*], M. Fernández-García [a], L.A. Pérez-Estrada [b], S. Malato [b]

[a] *Instituto de Catálisis y Petroleoquímica, CSIC. C/Marie Curie No. 2, Cantoblanco, 28049 Madrid, Spain*
[b] *Plataforma Solar de Almería-CIEMAT, Ctra.de Senés s/n, 04200 Tabernas, Almería, Spain*

Available online 6 August 2007

Abstract

The solar light photocatalytic degradation of ethidium bromide (EtBr) in aqueous suspensions has been analyzed over titania-based catalysts. A nanosized titania and an iron-doped TiO_2 (with ≈2 wt.% of iron content), synthesized within reverse microemulsions, were compared with a commercial Degussa P-25 titania. Structural and/or light handling properties of a different nature arise upon doping the titania with iron. These include favoring a titania crystal phase transformation from anatase to rutile and lowering the band gap energy. Almost total degradation of EtBr upon solar light assisted photodestruction and with significant total organic carbon (TOC) removal can be achieved over the three studied catalysts although the highest mineralization activity is achieved over the P25 titania sample. The results evidence that heterogeneous photocatalysis can be a promising advanced oxidation process to treat diluted EtBr residues typically generated in biomedical and biomolecular laboratories.

Keywords: Solar light; Photocatalysis; Iron; Ethidium bromide; Titania; Anatase; Rutile

1. Introduction

Ethidium bromide (EtBr; 3,8-diamino-6-phenyl-5-ethylphenanthridinium bromide), a dark red crystalline compound soluble in water and moderately toxic, is widely employed for rapid visualization of nucleic acids in electrophoretic gels and commonly used in molecular biology research and typically disposed in dilute aqueous solutions. EtBr is a potent mutagen for which the Environmental Health & Safety advises a detoxification protocol [1], since earlier recommended oxidation by household bleach was recognized to lead to possible by-products that could be more hazardous than the EtBr itself [2]. In spite of the availability of different methods for the EtBr detoxification, like chemical degradation or extraction/absorption among others, total degradation seems to be difficult to attain since there still exist doubts on the toxicity level of generated by-products.

Alternative methods based on the degradation of organic molecules upon reaction with active hydroxyl radicals, known as advanced oxidation processes (AOPs) [3], and which show promising properties for the treatment of waste waters with relatively low organic pollutant concentration, could be best suited for the treatment of EtBr residues generated in biomedical and biomolecular laboratories. Among the different AOPs process, heterogeneous photocatalytic oxidation employing semiconductors excitable by solar light has received much attention in recent years for the purpose of purifying water or waste water from industries and households [4–6]. TiO_2 is considered one of the most efficient photocatalysts since it displays reasonable photoactivity while it is quite stable under typical reaction conditions [7]. However, TiO_2 can present relative low overall quantum efficiency when employing solar light as exciting source due to their relatively large band gap. In this respect, TiO_2 doping at low concentrations with some heterocations of transition metals can improve the solar light absorption efficiency, which could potentially enhance the photoactivity of the catalytic system; wide surveys of Ti–M mixed oxides employed as photocatalysts using UV light have been previously reported [8,9].

* Corresponding authors. Fax: +34 915854760.
E-mail addresses: abahamonde@icp.csic.es (A. Bahamonde), amartinez@icp.csic.es (A. Martínez-Arias).

0920-5861/$ – see front matter © 2007 Elsevier B.V. All rights reserved.
doi:10.1016/j.cattod.2007.06.051

Other approaches to increase the photoefficiency of TiO_2-related materials are based on the employment of nanostructured configurations of TiO_2 [10,11]. Nanosized materials can have enhanced photochemical properties with respect to bulk specimens because they minimize band bending, facilitating the presence of both types of charge carrier, electron and holes, at the surface of titania, which makes them readily available for both reductive and oxidizing steps of the photocatalytic process [12,13]. Among different techniques employed for the manufacture of oxide nanoparticles [14,15], the microemulsion method has shown to provide interesting properties in terms of chemical and morphological homogeneity [16,17]. In the present work, water in oil (reverse) microemulsions were used to synthesize different catalysts and their catalytic performances for solar light-assisted aqueous EtBr photodegradation under pilot plant conditions were examined in comparison with that of a TiO_2 reference (P25 from Degussa company). The study is intended to analyze the physicochemical properties of this type of materials which can be most relevant to the mentioned photocatalytic degradation.

2. Experimental

2.1. Catalyst synthesis

An iron-doped photocatalyst was prepared using a microemulsion preparation method by addition of titanium-tetraisopropoxide to a reverse microemulsion containing an aqueous solution of iron (III) nitrate nonahydrate (0.5 M) dispersed in *n*-heptane, using Triton X-100 (Aldrich) as surfactant and 1-hexanol as cosurfactant [18]. The resulting mixture was stirred for 24 h, centrifuged, decanted, rinsed with methanol and dried at 298 K for 12 h. Then, the amorphous mixed oxide was calcined for 2 h at 600 °C in air atmosphere. This sample will be referred to hereafter as TiO_2–2Fe (2.0 wt.% is the nominal iron loading employed). A TiO_2 catalyst was also prepared by the same method. A commercial titania Degussa P25 sample was employed as reference.

2.2. Characterization techniques

Chemical analyses of the iron in the samples were performed by inductively coupled plasma (OES–ICP) with a Perkin-Elmer Optima 3300DV Model.

Powder XRD patterns were obtained with a Siemens D-500 apparatus using nickel-filtered Cu Kα radiation operating at 40 kV and 40 mA, with a 0.04° step size and accumulating a total of 5 s per point. Particle size and microstrain analyses were made from the XRD measurements by employing Williamson–Hall plots [9,19]. For this and also to obtain lattice parameters, peaks were analyzed and fitted using a least-squares fitting program [19] while data from the standard card JCPDS (Joint Committee on Powder Diffraction Standards) of TiO_2 anatase (JCPDS 84-1286) are used to identify this phase. The phase contents of a determinate sample were calculated from the integrated intensities of anatase (1 0 1) and rutile (1 1 0) peaks, employing a method reported elsewhere [20].

The diffuse reflectance absorption spectra of the photocatalysts were recorded with a UV–vis Varian 2300 apparatus. Analysis of the band gap transitions of the samples were made using equations developed elsewhere [21].

Nitrogen adsorption–desorption isotherms and the specific surface areas were examined by the BET method [22] and measured at 77 K in a Micrometritics Tristar automatic apparatus on samples previously outgassed overnight at 413 K to a vacuum of $<10^{-4}$ Pa to ensure a dry clean surface free from any loosely held adsorbed species. Mesopore volumes were determined from the amount adsorbed at a relative pressure of 0.96 on the desorption branch of the isotherm, equivalent to the filling of all pores below 50 nm diameter, minus any microporosity previously determined from the corresponding *t*-plot. The porosity studies were completed by mercury intrusion porosimetry (MIP) using CE Instruments Pascal 140/240 and applying the Washburn equation assuming a cylindrical non-intersecting pore model [23], with the values recommended by the IUPAC of 141° and 484 mN m^{-1}, respectively, for the contact angle and surface tension of mercury, giving data corresponding to pores from about 300 μm down to 7.5 nm diameter. The total pore volume was evaluated by combining the results of both techniques.

Ammonia adsorption at room temperature (measured on a Micromeritics ASAP-2010C instrument) was used to evaluate the surface acidity, expressed as mequiv. of ammonia adsorbed per gram of sample. The samples were first outgassed at 350 °C for 2 h, and then cooled to 30 °C before adsorbing ammonia to determine the physisorption plus chemisorption capacity. Subsequently, after outgassing the samples at 30 °C for 4 h to remove the physisorbed gas, a second adsorption process was carried out to obtain the chemisorbed amount by difference between the two isotherms.

2.3. Photoactivity studies

Photoreactors based on compound parabolic collectors (CPCs) from the Plataforma Solar de Almería (PSA) were employed to study the solar light photodegradation of EtBr. The static collectors present a reflective surface constituted by two connected parabolic mirrors with an absorber tube in the focus, which provide the most efficient light-harvesting optics for low concentration systems [24]. One advantage of CPC reactors is that the whole solar radiation reaching the collectors (both direct and diffuse) can be potentially collected by the reflector mirrors [25].

Waste water circulates under turbulent flow conditions inside the CPC absorber tubes within a closed recirculating system. The hydraulic circuit of the photoreactor is formed by a continuously stirred tank, a re-circulation pump and a solar collector which consists in three CPC modules arranged in series and placed on fixed supports inclined 37° (latitude of PSA) with respect to the horizontal plane. The plant is designed for operation in batch mode. The total volume in the experiments was 35 L and the volume irradiated in the solar collector was 22 L. A detailed description of the characteristics of the materials and components used in this set-up is given

elsewhere [26]. The starting conditions were the following: 20 mg L^{-1} of EtBr and 200 mg L^{-1} of catalyst, added to the 35 L stirred tank.

Evaluation of weather conditions was absolutely necessary to normalize the intensity of the solar irradiance. For this purpose, a Kipp&Zonen CUV3 broadband UV radiometer with UV range (285–400 nm) was used to determine the irradiance power in order to normalize runs carried out in different days. It was inclined 37° (local latitude in PSA) and oriented to the equator like the CPC photoreactor. A normalized illumination time defined elsewhere [27] was selected to standardize the solar irradiation. In this approach, the average solar UV flux on a perfect sunny day is considered as 30 W_{UV} m^{-2}; accordingly, the irradiation time will be represented as t_{30w}.

The total organic content (TOC) of aqueous samples was determined with a Shimadzu TOC-5050A analyzer equipped with a Shimadzu ASI-5000A autosampler. EtBr concentrations were monitored by high performance liquid chromatography with UV detection (HPLC-UV) at 285 nm, employing a nucleosil C-18 column at 50 °C and ammonium acetate/CAN at 65/35 ratio, respectively. Additional measurements of the EtBr concentration were done by means of a UV–vis Unicam-III spectrophotometer, for which small portions of the solutions were extracted along time.

The concentrations of short-chain organic acids and bromide formed during the photocatalytic process were measured with a Dionex DX-600 chromatograph, using a Dionex Ionpac AS11-HC 4× 250 mm anion column. The ammonium content was measured with a Dionex DX-120 chromatograph with a Dionex Ionpac CS12A 4× 250 mm cation column.

In turn, measurements of iron lixiviates to the reaction medium were made by OES-ICP with a Perkin-Elmer Optima 3300DV Model and revealed the absence of appreciable lixiviates under the employed conditions for TiO_2–2Fe.

3. Results and discussion

3.1. Characterization studies

Table 1 summarizes some physico-chemical properties of the studied catalysts. It can be observed that the iron content determined by chemical analysis of the titania doped catalyst (TiO_2–2Fe) is lower than the nominal iron content employed for its preparation (2 wt.%). The fact that only around 80% of the nominal iron content is incorporated to the sample has been also observed when other preparation methods are used [28,29]. It can be related to an incomplete iron trapping during the titanium isopropoxide hydrolysis process and the sweeping out of the weakly retained iron cations during the step of rinsing with methanol included to remove the solvents employed to make the reverse microemulsion.

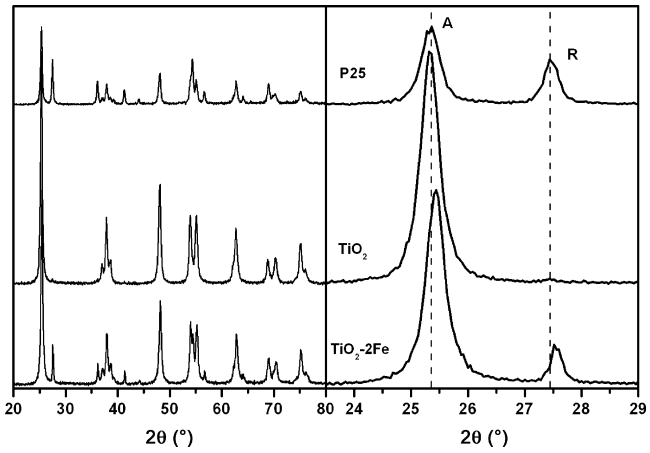

Fig. 1. XRD patterns of the indicated catalysts. A and R denote peaks characteristic of anatase and rutile, respectively.

X-ray patterns of the three catalysts are shown in Fig. 1. All of them display peaks belonging to anatase (tetragonal D_{4h}, *I*41/*amd*) and rutile (tetragonal C_{2v}, *P*42/*mnm*) titania phases [30]. The calculated percentages of each phase are displayed in Table 2 along with some structural parameters extracted from the XRD results. Since no hint of iron-containing segregated phases could be resolved from the TiO_2–2Fe pattern, it can be suggested that the iron must be relatively well dispersed in the catalyst. Some appreciable changes are apparent upon iron incorporation to the titania structure. First, in agreement with results in the literature [31], a phase transformation from anatase to rutile appears favored by the presence of iron and associated to an apparent increase of the anatase crystal size [10,31].

A small lattice contraction associated to a decrease of the c parameter of the anatase tetragonal cell was also observed upon iron incorporation (Table 2). A similar result was observed in previous investigations on other Fe-doped titania samples [31]. It can be noted that this effect is opposite to that found for other Fe-doped samples of this type, in which only the anatase phase was found as a consequence of application of lower calcination temperatures during the sample preparation (leading to appreciably lower primary particle sizes) [32]. In that case, a lattice expansion was detected upon iron incorporation, which was suggested to result from compensating effects between the incorporation of iron cations into substitutional positions of the anatase lattice (note that Fe^{3+} shows a similar, only slightly

Table 1
Physico-chemical properties of the studied catalysts

Catalyst	Fe content (wt.%)	Acidity (mmol g^{-1})[a]	Textural properties			Band gap (eV)	
			S_{BET} (m^2 g^{-1})	V_{Total} (cm^3 g^{-1})	$d_{mesopore}$ (nm)	Direct transition	Indirect transition
P25	–	0.08	48	0.000	–	3.40	2.90
TiO_2	–	0.10	20	0.080	9.8	3.18	2.89
TiO_2–2Fe	1.62	0.19	26	0.054	4.8	2.92	2.17

[a] From NH_3 chemisorption results.

Table 2
XRD derived characteristics of the titania-based catalysts

Catalyst	*c* parameter[a]	Cell volume[a] (Å^3)	Crystal size (nm)	Microstrain[a]	Anatase (%)	Rutile (%)
P25	9.500	136.0	25	1.31×10^{-3}	66	34
TiO_2	9.507	136.3	21	0.76×10^{-3}	100	0
TiO_2–2Fe	9.480	135.5	37	2.45×10^{-3}	90	10
Anatase card (JCPDS 84-1286)	9.505	136.0				

[a] For the anatase phase.

lower, ionic radius than Ti^{4+}) and oxygen vacancy generation for maintenance of charge neutrality [32,33]. In this sense, the anatase contraction observed for TiO_2–2Fe (Table 2) can be related to the incorporation of iron to other sites of the lattice, like interstitial ones. Such iron incorporation has been proposed to occur in a previous report in which certain lattice contraction was also detected [31].

Another apparent effect of iron incorporation into the anatase lattice is related to the increase detected in the lattice microstrain (Table 2), similar to observations reported for W-doped titania [9]. This effect appears also opposite to that observed for iron-doped samples of lower particle size and displaying anatase as unique phase [32], suggesting again a difference in the anatase sites at which iron can be preferentially incorporated in each case. It must be noted that the differences in the iron configuration present in each case can be most relevant to explain differences in the photocatalytic properties of this type of samples [7,34].

UV–vis spectra of the samples are displayed in Fig. 2. The sharp increase of the absorption spectra at wavelength lower than 380 nm (ca. 3.2 eV) can be assigned to the intrinsic band-gap absorption of pure anatase TiO_2 [22]. The presence of iron shifts the absorption threshold onset to the visible region above 400 nm which could in principle result beneficial to improve the photoactivity under solar light excitation. Apparently two components contribute to this enhanced absorption in the visible region. One can be attributed to the excitation of 3d electrons of Fe^{3+} to the TiO_2 conduction band (charge transfer transition), which gives rise to a band centred at ca. 400 nm [33,35]. Second, a band centred at ca. 500 nm can be ascribed to the d–d transition

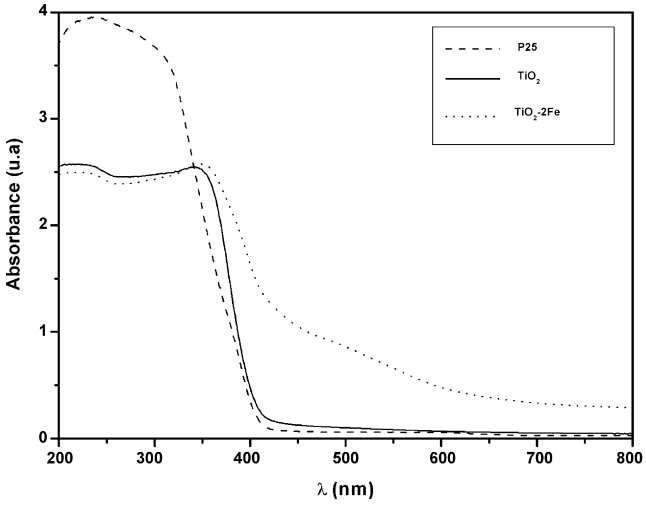

Fig. 2. UV–vis spectra for the indicated catalysts.

of Fe^{3+} ($^2T_{2g} \rightarrow {}^2A_{2g}$, $^2T_{1g}$) or the charge transfer transition between interacting iron ions ($Fe^{3+} + Fe^{3+} \rightarrow Fe^{4+} + Fe^{2+}$) into small oxidic iron clusters [32,33]. An analysis of the band gap transitions is also shown in Table 1, indicating the character (direct or indirect) of identified electronic transitions.

The textural properties of the examined catalysts are summarized in Table 1. Relatively low surface areas were found in all cases. In spite of this, noteworthy the presence of certain mesopority is appreciated for TiO_2 or TiO_2–2Fe samples while the iron doping apparently leads to a lower mesopore average diameter. Besides, a bimodal pore size in the range of meso and macroporosity was also found for these two samples. On the other hand, nitrogen adsorption–desorption isotherms for TiO_2 and TiO_2–2Fe (not shown) corresponded to type IV isotherms, characteristic of many inorganic oxide gels [36].

Concerning surface acidity (expressed as micromoles of NH_3 chemisorbed per gram of sample, see Table 1), all the studied catalysts presented relatively low values, although a slight increase was observed for the iron-doped titania catalyst, in agreement with previous observations for other catalysts of this type [32].

3.2. Photocatalytic tests

Fig. 3a displays the influence of normalized solar irradiation time on EtBr evolution for the three examined catalysts. It can

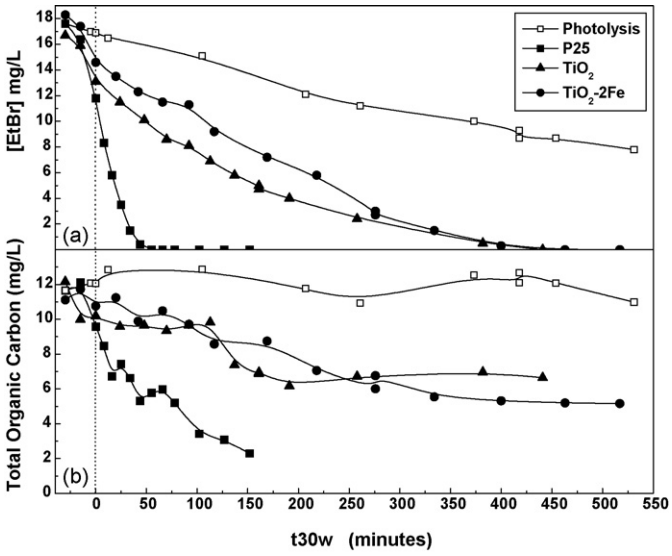

Fig. 3. (a) EtBr evolution (HPLC-UV detection) during the course of the photocatalytic runs over the indicated catalysts. (b) Total organic carbon evolution during the photocatalytic runs.

be noted that some decrease of the EtBr concentration is detected in the dark although no important TOC decrease is observed before irradiation (Fig. 3b). This suggests that a small preliminary EtBr degradation can take place as a consequence of EtBr interaction with the catalysts while independent experiments (not shown) reveal that the EtBr chemisorption prior to irradiation is almost negligible for any of the three catalysts. A blank run in the absence of catalyst was carried out under the same operating conditions. This reveals that a certain photolysis degradation of EtBr takes place under the employed conditions, which confirms the unstable character of this mutagenic pollutant under solar light irradiation. However, since no TOC evolution is detected as a consequence of this EtBr photolysis, it is clear that the EtBr degradation observed during the heterogeneous photocatalytic process can be directly attributed to the generation of reactive species (like hydroxyl radicals, $OH^{\bullet}$) upon excitation of the TiO_2-based photocatalysts.

A very important decrease of EtBr concentration is observed from the beginning of the run with commercial P25 titania, resulting in total conversion after about 50 min of normalized irradiation time. In contrast, a lower EtBr removal rate is detected when using the home made titania catalysts (TiO_2 and TiO_2–2Fe), with which total EtBr degradation can also be attained after about 400 min of normalized irradiation.

The results for TOC evolution during EtBr photodegradation with the three studied catalysts are displayed in Fig. 3b. It is noted that a significant TOC reduction (≈80%) was only obtained with the P25 titania after about 150 min of irradiation. In contrast, a more moderate TOC conversion (lower than about 60%), was attained with TiO_2 and TiO_2–2Fe.

These results evidence that the introduction of iron inside the titania structure does not appreciably improve the photoassisted EtBr degradation. In spite of its higher specific area (Table 1) almost the same total EtBr conversion and TOC removal is achieved over the iron-doped system (TiO_2–2Fe) in comparison with the iron-free one (TiO_2). From literature studies it is known that detrimental effects on the photoactivity can arise upon iron doping of titania as a consequence of specific iron configurations acting as charge recombination centres [34]. Thus, the beneficial effect on the generation of charge photocarriers of the extension of the light absorption to the visible region observed in the presence of iron (in accordance with UV–vis results of Fig. 2) appears compensated by a relatively faster destruction of such photocarriers as a consequence of the mentioned e^-/h^+ recombination process.

3.3. Mechanistic aspects

Hints on the differences in the EtBr photodegradation rates between the catalysts can be obtained upon analysis of the evolution of short chain organic acids in comparison with the TOC evolutions observed. Fig. 4 displays the evolution of the short organic acids in function of irradiation time for these three studied catalysts. The main short-chain organic acid detected was maleic acid although some traces of oxalic, acetic and formic acids were also formed. In this sense, the TOC residual remaining after about 150 min of irradiation time when

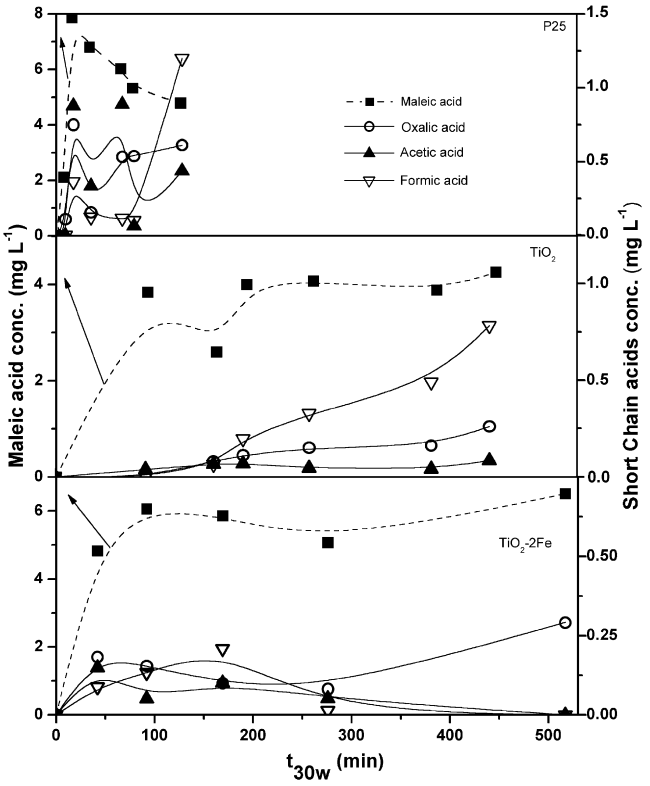

Fig. 4. Evolution of short chain organic acids during the course of the photocatalytic runs for the indicated catalysts.

P25 titania is employed can perfectly correspond to the presence of these short organic acids, fundamentally maleic acid which shows to be somewhat more resistant to further photooxidation (Fig. 4). However in the case of the other two photocatalysts, a lower short organic acid concentrations is detected which cannot be correlated with the relatively large TOC content remaining in the system after prolonged irradiation (Figs. 3 and 4). This result points towards the presence of other different by-products or molecules which appear more difficult to degrade by photocatalysis and which can be complex to detect by the used analytical techniques.

In this respect, an independent monitoring of the evolution of the EtBr concentration during the course of the photocatalytic runs by employing UV–vis spectroscopy detection has been performed, in which (in contrast to the HPLC-UV detection) a whole UV–vis spectra of a portion of solution extracted from the reaction medium (see Section 2) is analysed. The EtBr solved in water displays four transitions: one in the visible region at 480 nm, a strong transition at 285 nm which present a shoulder at 343 nm and a far UV transition at 210 nm. Hundson and Jacobs have studied the electronic transitions of EtBr [37]. These authors have observed a strong similarity between the transitions of EtBr and phenantrene in terms of both the position and intensity of the bands. This is not unexpected considering that both molecules present strong structural similarities, taking into account that phenantridinium is derived from phenantrene by replacement of a carbon by a nitrogen atom in the nine position and the fact that such substitution with a quaternary nitrogen has little effect on the

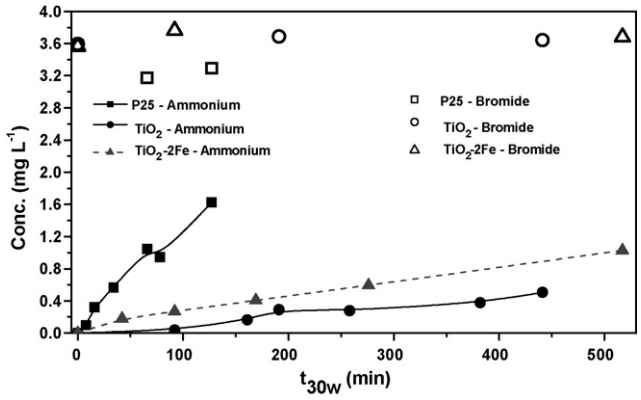

Fig. 5. Evolution of bromide and ammonium during the course of the photocatalytic runs for the indicated catalysts.

transitions [37]. A similar absence of changes in the electronic transitions has been also observed when there are changes in some of the substitutional groups of the phenathrene or phenantridinium molecule. Therefore, the transitions of EtBr are not severely affected upon removal of the phenyl or amino groups which are bonded to the phenantridinium structure of EtBr [37]. It can therefore be proposed that the decrease in the intensity of UV bands of EtBr during the photocatalytic process (Fig. 3a) reveals the rupture of the phenanthridinium ring. Nevertheless, fragments corresponding to the substitutional external groups (phenyl, amino-containing organic molecules, etc.) escaping detection by the employed techniques can remain in the reaction medium and be responsible for the relatively large TOC content still remaining at the end of the photocatalytic runs over TiO_2 and TiO_2–2Fe samples (Fig. 3b).

Finally, the bromide evolution remained almost constant, 3.2–3.6 mg L^{-1}, along irradiation time for the three studied catalysts (Fig. 5). In turn, the ammonium concentration slightly increased during the course of the EtBr photodegradation process with all the studied catalysts (Fig. 5). A particularly high increase was detected for the P25 titania catalyst, which generates almost 2 ppm at longer times, in agreement with the highest TOC removal produced in the presence of this photocatalyst (Fig. 3b).

4. Conclusions

Appreciable structural modifications are produced in titania upon iron doping. Among them, rutile formation along with an apparent increase of primary crystal size is shown to be favored by the presence of this transition metal. The structural parameters observed for TiO_2–2Fe suggest that at least a part of the iron can be incorporated to interstitial sites of the anatase lattice. In turn, as expected, the presence of iron shifts the absorption spectrum to the visible region. However, no important improvement in the EtBr photodegradation with solar light is apparent for the iron-doped sample, which suggests that some iron cations in the sample could act as recombination centers, compensating the beneficial effect of the improved visible light absorption. Nevertheless, total EtBr degradation can be achieved with home made TiO_2 and iron-doped TiO_2 although the highest degradation rate, with significant TOC removal, is only achieved when using commercial Degussa P25 titania. To conclude, photocatalysis employing solar light is shown to be a promising advanced oxidation process to remove EtBr disposals from waste waters.

Acknowledgements

C.A. would like to thank the Spanish Ministry of Education and Science (Programa de Acceso de Grandes Instalaciones Científicas Españolas GIC-05-17) and the PhD Program of Autonoma University of Madrid, for financial support. Financial support by CSIC (project PIF 200420F0280) and MEC (CTQ2006-15600/BQU) is appreciated. We also appreciate the technical assistance of Agustín Carrión.

References

[1] Enviromental Health & Safety. University of California at Irvine. (http://www.ehs.uci.edu).
[2] G. Lunn, E.B. Sansone, Anal. Biochem. 162 (1987) 453.
[3] O. Legrini, E. Oliveros, A.M. Braun, Chem. Rev. 93 (1993) 671.
[4] I. Akmehmet, I. Arslan, Environ. Pollut. 103 (1998) 261.
[5] C. Hachem, F. Bocquillon, O. Zahraa, M. Bouchy, Dyes Pigments 49 (2001) 117.
[6] S. Malato, J. Blanco, A. Vidal, C. Richter, Appl. Catal. B 37 (2002) 1.
[7] M.R. Hoffmann, S.T. Martin, W. Choi, D. Bahnemann, Chem. Rev. 69 (1995) 95.
[8] W. Choi, A. Termin, M.R. Hoffman, Angew. Chem. Int. Ed. 33 (1994) 1091.
[9] M. Fernández-García, A. Martínez-Arias, A. Fuerte, J.C. Conesa, J. Phys. Chem. B 109 (2005) 6075.
[10] M. Fernández-García, A. Martínez-Arias, J.C. Hanson, J.A. Rodriguez, Chem. Rev. 104 (2004) 4063.
[11] D.-H. Chen, S.-H. Wu, Chem. Mater. 12 (2000) 1354.
[12] W. Choi, A. Termin, M.R. Hoffmann, J. Phys. Chem. 98 (1994) 1369.
[13] A.J. Maira, K.L. Yeung, J. Soria, J.M. Coronado, C. Belver, C.Y. Lee, V. Augugliaro, Appl. Catal. B 29 (2001) 327.
[14] R.W. Siegel, J. Mater. Res. 3 (1998) 1367.
[15] P. Fayet, L.Z. Woste, Phys. D. 3 (1986) 177.
[16] M. Boutonnet, J. Kizling, P. Stenius, G. Marie, Coll. Surf. 5 (1982) 209.
[17] M.P. Pilen, Langmuir 13 (1999) 3266.
[18] A. Martínez-Arias, M. Fernández-García, V. Ballesteros, L.N. Salamanca, J.C. Conesa, C. Otero, J. Soria, Langmuir 15 (1999) 4796.
[19] A. Weibel, R. Bouchet, F. Boulch, P. Knauth, Chem. Mater. 17 (2005) 2378.
[20] H. Zhang, J.F. Banfield, J. Phys. Chem. B 104 (2000) 3481.
[21] N. Serpone, D. Lawless, R. Khairutdinovt, J. Phys. Chem. 99 (1995) 1646.
[22] S. Brunauer, P.H. Emmett, E. Teller, J. Am. Chem. Soc. 60 (1938) 309.
[23] R.I. Bickley, T. Gonzalez Carreño, J.S. Lees, L. Palmisano, R.J.D. Tilley, J. Sol. State Chem. 92 (1991) 178.
[24] J. Muschaweck, W. Spirkl, A. Timinger, N. Benz, M. Dörfler, M. Gut, E. Kose, Solar Energy 68 (2000) 151.
[25] S. Malato, J. Blanco, M.I. Maldonado, P. Fernández, D. Alarcón, M. Collares, J. Farinha, J. Correia, Solar Energy 77 (2004) 513.
[26] M. Kositzi, A. Antoniadis, I. Poulios, I. Kiridis, S. Malato, Solar Energy 77 (2004) 591.
[27] M. Hincapié Pérez, G. Peñuela, M.I. Maldonado, O. Malato, P. Fernández-Ibañez, I. Oller, W. Gernjak, S. Malato, Appl. Catal. B. 64 (2006) 272.

[28] X. Li, P.-L. Yue, C. Kutal, New J. Chem. 27 (2003) 1264.
[29] D. Cordischi, N. Burriesci, F. D'Alba, M. Petrera, G. Polizzoti, M. Schiavello, J. Solid State Chem. 56 (1985) 182.
[30] J.K. Burdett, T. Hughbanks, G.J. Miller, J.W. Richardson Jr., J.V. Smith, J. Am. Chem. Soc. 109 (1987) 3639.
[31] J.A. Wang, R. Limas-Ballesteros, T. López, A. Moreno, R. Gómez, O. Novaro, X. Bokhimi, J. Phys. Chem. B 105 (2001) 9692.
[32] C. Adán, A. Bahamonde, M. Fernández-García, A. Martínez-Arias, Appl. Catal. B. 72 (2007) 11.
[33] J. Zhu, F. Chen, J. Zhang, H. Chen, M. Anpo, J. Photochem. Photobiol. A 180 (2006) 196.
[34] M.I. Litter, J.A. Navío, J. Photochem. Photobiol. A 98 (1996) 171.
[35] T. Umebayashi, T. Yamaki, H. Itoh, K. Asai, J. Phys. Chem. Sol. 63 (2002) 1909.
[36] F. Rouquerol, J. Rouquerol, K. Sing, Adsorption by Powders & Porous Solids. Principles, Methodology and Applications. Ed., Academic Press, 1999, pp. 323.
[37] B. Hundson, R. Jacobs, Biopolymers 14 (1975) 1309.